Geothermics 134 (2026) 103531

Contents lists available at ScienceDirect

Geothermics

journal homepage: www.elsevier.com/locate/geothermics

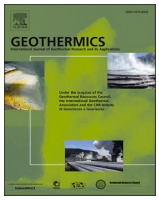

Application of the Monte Carlo method for geothermal resource assessment in low-exploration, high-potential areas: A case study of the Longchuan Basin, Southwest China

Xiaoxue Jiang [a,b], Chuanqing Zhu [a,b,*], Fang Xie [a,b], Yuanjin Sun [a,b], Qian Cao [c], Dong Sun [d], Chaohe Fang [e], Yonghui Huang [a,b], Yaodong Xu [a,b]

[a] State Key Laboratory of Deep Geothermal Resources, China University of Petroleum (Beijing), Beijing 102249, China
[b] College of Geosciences, China University of Petroleum (Beijing), Beijing 102249, China
[c] PetroChina Research Institute of Petroleum Exploration and Development, Beijing 100083, China
[d] PetroChina Research Institute of Petroleum Exploration and Development-Northwest, Gansu 730020, China
[e] PetroChina Shenzhen New Energy Research Institute Co. Ltd., Shenzhen 518063, China

ARTICLE INFO

Keywords:
Geothermal resources
Monte Carlo simulation
Resource uncertainty
Low-exploration area
Longchuan Basin

ABSTRACT

The Longchuan Basin, located in the high-temperature geothermal zone of the Mediterranean-Himalayan region, exhibits significant geothermal potential due to intense tectonic activity and a high heat flow background. However, limited exploration and insufficient data have hindered accurate resource assessment. In this study, reliable heat flow values were obtained through systematic drilling temperature measurements and core thermal property analysis, clarifying the spatial distribution of the basin's temperature field. Using the Monte Carlo volumetric method, key reservoir parameters such as temperature, thickness, and porosity were modeled to quantify the uncertainty of geothermal resource estimates. Results show an average geothermal gradient of 3.87 °C/100 m and surface heat flow ranging from 70 to 90 mW/m^2. The hydrothermal resource potential is characterized by a P10 of 4.10 × 10^{14} KJ, a P50 of 8.87 × 10^{14} KJ, and a P90 of 1.59 × 10^{15} KJ. For hot dry rock resources, the P10, P50, and P90 values are 1.21 × 10^{16} KJ, 1.32 × 10^{16} KJ, and 1.43 × 10^{16} KJ, respectively. Compared with conventional methods, the Monte Carlo approach effectively captures parameter uncertainty, improving assessment reliability. This study provides a methodological reference for geothermal exploration in under-explored basins with high geothermal potential.

1. Introduction

Under the dual pressures of the global energy crisis and environmental pollution, the development of clean and renewable energy sources has become increasingly urgent. Among them, geothermal energy has attracted significant attention due to its abundant reserves, sustainability, and low carbon emissions (Carlino et al., 2012; Bahadori et al., 2013; Wang et al., Zhang and Hu, 2018). The Yunnan-Tibet geothermal zone is part of the Himalayan high-temperature geothermal belt, located within the main collision zone between the Indian and Eurasian plates. Intense tectonic activity in this region has induced widespread modern hydrothermal systems (Tong and Zhang, 1981; Shangguan et al., 2005; Wu et al., 2023; Zeng et al., 2025). The Longchuan Basin, situated in the south-central segment of the Sanjiang orogenic belt in Dehong Prefecture, Yunnan Province, is characterized by well-developed fault systems, active magmatism, and prominent high-temperature geothermal manifestations, providing favorable conditions for geothermal resource accumulation (Zhang et al., 1987; Huang et al., 2020). Previous studies have analyzed the geothermal geological background, hydrothermal activity, and hydrochemical characteristics of this area, and preliminarily summarized the formation conditions of geothermal resources in specific zones (Liu et al., 2015; Duan et al., 2019; Wu et al., 2021). These findings provide a valuable foundation for subsequent quantitative evaluation of geothermal resources in the region. In the early stages of geothermal resource assessment, evaluations primarily relied on analogy-based methods, where the potential of a target area was inferred from developed geothermal fields. These approaches were highly subjective and

* Corresponding author at: State Key Laboratory of Petroleum Resources and Engineering, China University of Petroleum (Beijing), Beijing 102249, China.
E-mail address: zhucq@cup.edu.cn (C. Zhu).

https://doi.org/10.1016/j.geothermics.2025.103531
Received 31 March 2025; Received in revised form 6 November 2025; Accepted 12 November 2025
Available online 19 November 2025

exhibited significant regional dependence. Subsequently, the heat flow density method became the first widely adopted systematic quantitative approach in thermal anomaly zones (Banwell, 1963; Muffler and Cataldi, 1978). Other approaches, including magmatic heat budget estimation and planar fracture conduction models, were also explored (Noguchi, 1970; Bodvarsson, 1974), but their practical applications remained limited.

To meet the growing demand for quantitative geothermal evaluation—particularly by the United States Geological Survey (USGS)—Muffler and Cataldi (1978) systematically introduced the volumetric method, which estimates recoverable thermal energy based on parameters such as reservoir area, thickness, temperature, porosity, heat capacity, and recovery factor. Owing to its conceptual simplicity and limited data requirements, the volumetric method has been extensively applied in preliminary assessments worldwide, including Cornwall in the UK, various geothermal fields in Mexico, and the Bohai Bay Basin in China (Turan et al., 2024; Palacios et al., 2024; Rao et al., 2023; Chen et al., 2024).With advancements in computational capabilities, numerical simulation techniques began to mature in the 1980s and are now widely used during the middle to late stages of geothermal development (O'Sullivan et al., 2001). However, the application of these methods is often constrained by limited data on subsurface structure, thermal properties, and fluid flow boundaries in early-stage exploration areas. Consequently, the volumetric method remains the most commonly adopted approach in low- to medium-exploration contexts due to its practicality and adaptability.

Traditional volumetric estimates often rely on fixed parameter values, which may not reflect spatial variability in key geological characteristics such as temperature, reservoir thickness, and porosity. This can result in substantial uncertainties. To address this issue, recent studies have combined the volumetric method with Monte Carlo simulations. This integration enables probabilistic sampling and statistical evaluation of key parameters, resulting in resource estimates expressed as probability distributions with quantified uncertainty (Garg and Combs, 2015; Piris et al., 2021; Fariña-González et al., 2025), thereby improving the reliability of geothermal resource assessments.

The Longchuan Basin in southwestern China was selected as a case study. Based on regional geological conditions, borehole temperature measurements, and thermal property data, a reservoir–caprock configuration model was constructed. A Monte Carlo–based volumetric method was then applied to assess the geothermal potential of both hydrothermal and hot dry rock systems. The results offer technical insights and scientific support for geothermal exploration in the Longchuan Basin and other low-exploration areas with favorable thermal regimes.

2. Geological setting

The Longchuan Basin is a small fault basin located on the Tengchong Block, and together with nearby basins such as the Yingjiang Basin and Lianghe Basin, it is referred to as the Western Yunnan Basin Group. The Tengchong Block is located within the collision zone between the Gondwana-derived Indian Plate and the Eurasian Plate (Yangtze Block), forming an essential part of the eastern Tethyan tectonic belt. It is bounded to the east by the Gaoligongshan shear zone and to the west by the Myitkyina–Sagaing Fault and the Mogok Metamorphic Belt, which separate it from the Burma Massif (Li et al., 2011). Since approximately 55 Ma, the ongoing collision between the Indian and Eurasian plates, coupled with regional clockwise rotation, subduction rollback, and complex tectonic evolution, has significantly modified the lithospheric structure of the Tengchong Block. Under a regional NW-directed extensional stress regime, the block experienced crustal extension and lithospheric thinning, which facilitated upwelling of asthenospheric material and triggered extensive magmatic activity. This process led to the development of active volcanic groups and large-scale crust-mantle magmatic bodies, such as the magma chamber buried at a depth of 5–8 km in the adjacent Yingjiang Basin, resulting in pronounced thermal anomalies. Additionally, NE and NS strike-slip fault systems developed under regional compressive stress, leading to the formation of multiple pull-apart basins in the area (Fig. 1) (Chen et al., 2023; Gao et al., 2023).

As a result of these tectonic dynamics, the Longchuan Basin has undergone multiple stages of deformation, including an initial extension stage, a strike-slip stage with complex fault activity, and a final compressive adjustment stage (Chen et al., 1994; Huang et al., 2020). The basin, which has a northeast-southwest orientation, spans an area of approximately 475 km^2. Its stratigraphy includes Cambrian basement rocks, Neogene Nanlin and Mengbao formations, and Quaternary sediments. The basement rocks primarily consist of granite, gneiss, and marble, while the Neogene Nanlin Formation is mainly composed of sandstone, siltstone, and mudstone. The Mengbao Formation contains conglomerates and mudstones, with coal seams present in some areas. The Quaternary is characterized by yellowish-gray topsoil. The extensive distribution of Neogene and Quaternary cap beds provides essential conditions for the formation of geothermal resources in the Longchuan Basin (Zhang et al., 2021).

3. Geothermal field

3.1. Geothermal gradient

Based on the systematic temperature measurements and geothermal gradient data from Well L4X and Well L4AX, formation temperature generally shows a linear correlation with depth, though some discrepancies are observed. In the case of Well L4X, a temperature disturbance occurs at depths greater than 1500 m, causing a significant decrease in the geothermal gradient, indicative of a single thermal anomaly. However, Well L4AX experiences thermal disturbances in both the shallow (200–500 m) and deeper (1200–1800 m) sections, with a negative gradient of −4 °C/100 m observed in certain intervals (200–300 m). This 'negative geothermal gradient' in the shallow section is likely related to the recharge process of shallow groundwater. Low-temperature groundwater enters the formation through recharge and migrates downward. As it moves downward, it undergoes heat exchange with the warmer, deeper environment, resulting in cooling effects on the lower strata, which causes the temperature profile to shift toward lower temperatures.

Considering both wells are located near fault zones, it is hypothesized that the deep thermal disturbances in these wells may be linked to high-temperature upwelling. Specifically, deep high-temperature groundwater transports heat upward from the bottom layers, exchanging heat with relatively cooler shallow groundwater, thus heating the shallow groundwater. The region contains several hot springs, with an average wellhead temperature of 42 °C, further supporting the idea that the fault zone influences the shallow temperature (Zhang et al., 2021). This also suggests the potential for deep heat transfer through the fault zone. Additionally, the geothermal gradient varies across different well sections, likely due to differences in the lithological composition of the formations, which affects thermal conductivity. This variation in lithology, combined with the hydraulic characteristics of the fault zone, complicates the geothermal distribution in the area (Fig. 2).

3.2. Rock thermal properties

Previous studies on the thermal physical properties of rocks in the Longchuan Basin are limited. In this study, a total of 31 rock samples were collected from Wells L4X and L4AX. The sampled horizons covered Neogene and Paleogene strata, and the rocks were primarily composed of coarse sandstone, siltstone, argillaceous sandstone, mudstone, and metamorphic rocks. The transient plate heat source method was used to measure the thermal conductivity of the core samples. The distribution range of the obtained data is shown in Fig. 3.

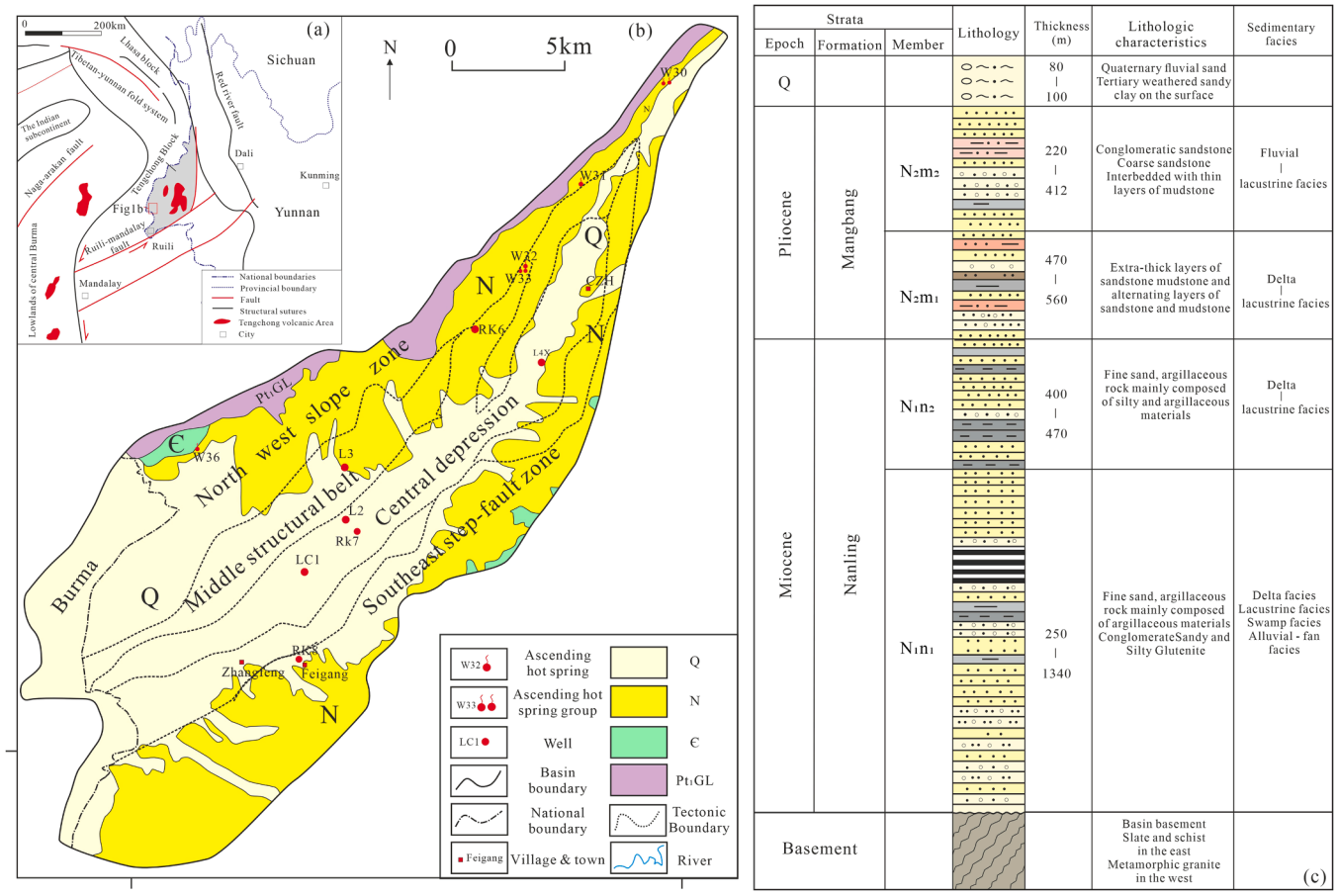

Fig. 1. Tectonic division in the study area and integrated stratigraphic column.

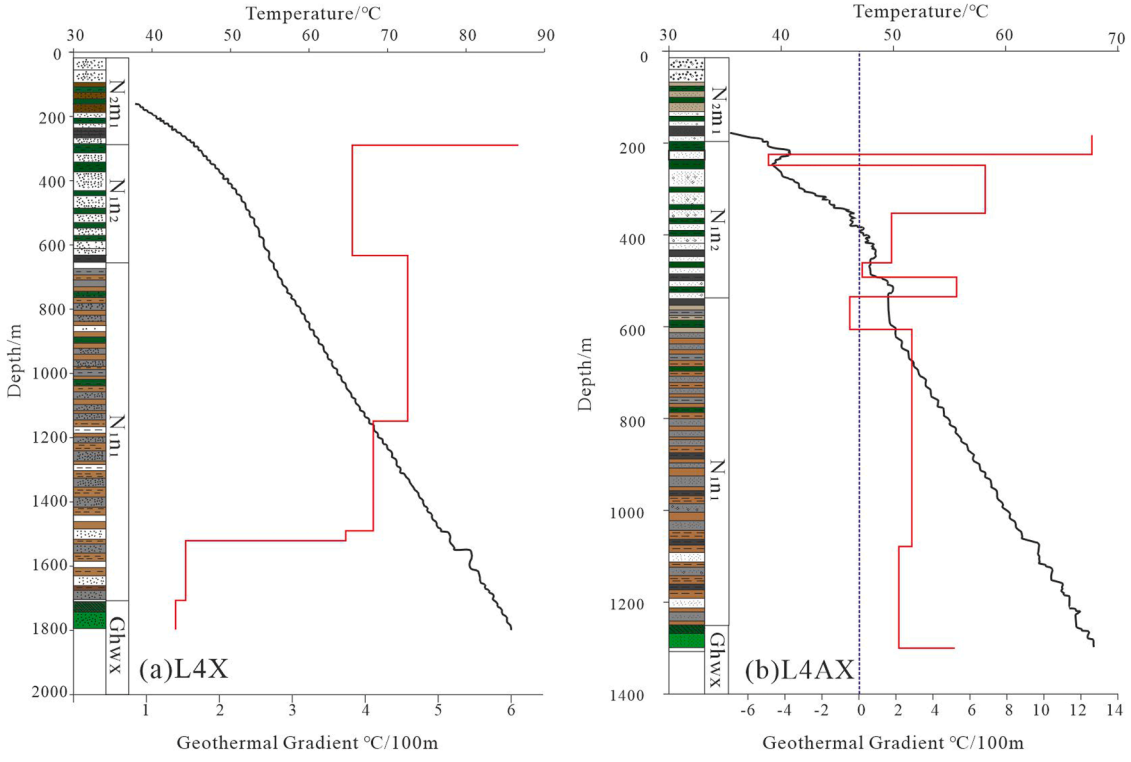

Fig. 2. System temperature measurement wells. (a) L4X well. (b) L4AX well. (The black line represents temperature, and the red line represents the geothermal gradient.).

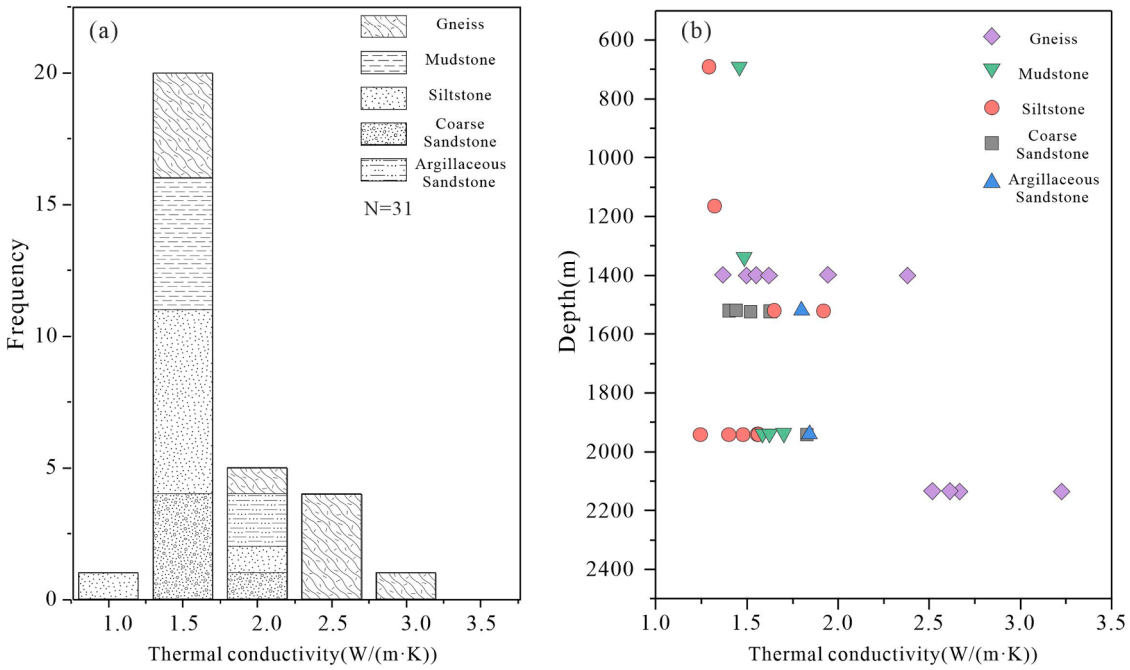

Fig. 3. Thermal conductivity frequency distribution diagram(a) and thermal conductivity-depth variation diagram (b).

The thermal conductivity in the Longchuan Basin ranges from 1.24 to 3.23 W/m·K, with an average of 1.75 W/m·K. The thermal conductivity of gneiss ranges from 1.37 to 3.23 W/m·K, with an average of 2.14 W/m·K. The thermal conductivity of mudstone ranges from 1.46 to 1.70 W/m·K, with an average of 1.57 W/m·K. For sandstone, the thermal conductivity ranges from 1.24 to 1.92 W/m·K, with an average of 1.49 W/m·K. The thermal conductivity of coarse sandstone ranges from 1.40 to 1.83 W/m·K, with an average of 1.56 W/m·K. The average thermal conductivity of shaly sandstone is 1.82 W/m·K. Additionally, while the thermal conductivity of siltstone and argillaceous sandstone shows no significant change trend with depth, the thermal conductivity of gneiss increases with depth.

The radioactive heat generation rate of rock refers to the energy released by the decay of radioactive elements per unit volume of rock per unit time and is a key parameter in studying the thermal state of deep basins. In practice, the contents of uranium (U), thorium (Th), and potassium (K) in rock samples are typically measured, and established calculation methods are used for estimating the heat generation rate. The formula by Rybach (1976) is one of the most widely applied:

$$A = 0.01\rho(9.52C_u + 2.56C_{Th} + 3.48C_k) \quad (1)$$

Where: A is the radioactive heat generation rate of rock (μW/m^3), ρ is the rock density (g/cm^3); Cu,Cth and Ck are the contents of uranium, thorium, and potassium in the rock, in μg/g, μg/g, and %, respectively.

Gamma logging is employed to measure the total gamma ray intensity produced by the decay of radioactive elements in formation rocks. The higher the concentration of the respective elements, the higher the intensity of gamma rays. In 1996, Bucker and Rybach proposed a linear relationship between the gamma logging curve value and the heat generation rate A, based on the sensitivity of gamma logging to U, Th, and K. This allows the heat generation rate to be calculated directly from the gamma logging data (Bücker & Rybach, 1996). The empirical formulas are:

$$A = 0.0158[\mathrm{GR(API)} - 0.8] \quad (2)$$

Through the correlation analysis of the natural radioactivity logging (natural gamma and natural gamma-ray spectrometry) data from 100 to 5000 m of the main borehole of the Chinese Continental Scientific Drilling (CCSD) and the measured heat generation rate data, a new GR-A linear relationship was established (Luo et al., 2008):

$$A = 0.0115(GR + 9.1) \quad (3)$$

In this research, gamma ray logging data from five wells in the basin were collected, and two empirical formulas were used to calculate the formation radioactive heat generation rate (Fig. 4). The results show that both methods exhibit the same general trend, with lower heat generation rates in the shallow formations and higher heat generation rates in the deeper Nanlin formation. Comparative analysis reveals that the heat generation rate calculated using formula (2) is lower than that calculated using formula (1). Specifically, the heat generation rate calculated by formula (1) primarily falls within the range of 1.5–3.5 μW/m^3, while that of formula (2) is concentrated between 1.0–2.5 μW/m^3.

To verify the reliability of the calculated results, the heat generation rate values obtained by the two methods were compared with 110 heat generation rate data points calculated by previous studies, which were based on the content of uranium (U), thorium (Th), and potassium (K) in western Yunnan (Li et al., 2011; Xiong et al., 2012; Wu et al., 2020; Zou et al., 2016; Liu and Liu, 2015). A total of 56,744 heat generation rate data points calculated using the empirical formula of Bücker and Rybach (1996) showed that the mean and standard deviation (2.72 ± 0.80 μW/m^3) closely matched the measured data (2.84 ± 1.19 μW/m^3) (Table 1), with similar frequency distribution characteristics (Fig. 5). This confirms that the formula is suitable for calculating the heat generation rate in the Longchuan Basin strata.

By measuring the thermal conductivity across the entire well section of the well L4X and well L4AX in the Longchuan Basin and calculating the heat generation rate based on the gamma ray logging data, this study establishes the thermal property profile for the region, providing crucial data support for subsequent geothermal field calculations (Table 2).

3.3. Heat flow

Based on system temperature measurements from Well L4X in the Longchuan Basin, the geothermal gradient of the stable section was determined, and the thermal conductivity of the core rock samples was measured, yielding high-quality (Grade A) heat flow data. In addition, the geothermal gradient of Well Lc1 was estimated using wellhead and

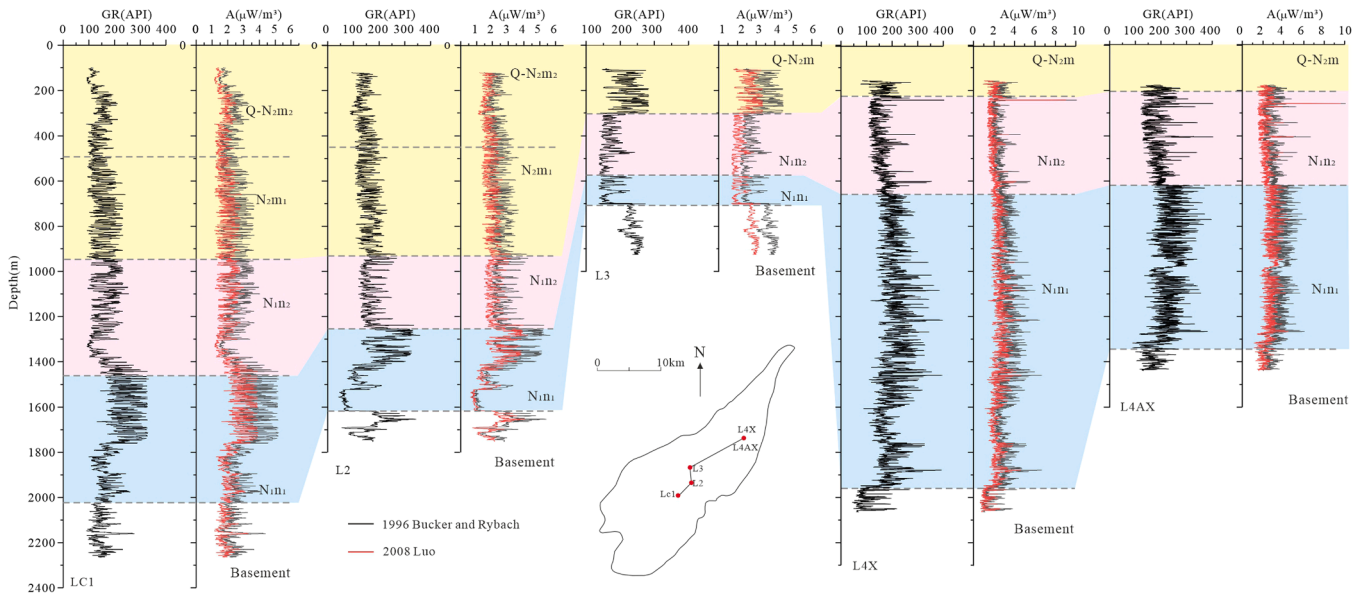

Fig. 4. Gamma-ray and heat generation rate curves for different logging curves in the Longchuan Basin.

Table 1
Comparison of the heat generation rate calculated using different GR - A empirical formulas with the measured heat generation rate.

Empirical relationship/ measurement	Bücker and Rybach (1996)	Luo et al. (2008)	Measured value
Mean value ($\mu W/m^3$)	2.72	2.09	2.84
Standard value ($\mu W/m^3$)	0.80	0.58	1.19

bottom-hole temperatures and, when combined with the thermal conductivity values from adjacent wells, produced Grade B heat flow data (Table 3). The Longchuan Basin, located in the southeastern part of the Tengchong Block in western Yunnan, lies at the forefront of the India–Eurasia collision zone and forms part of the Cenozoic Tengchong–Lianghe–Longchuan basin system. Given the limited exploration of this area, the heat flow database for the Longchuan Basin had previously been blank. The new data presented in this study fill a crucial gap, providing key baseline information for characterizing the regional geothermal field and improving the reliability of geothermal resource assessments. Based on these new measurements, together with the Compilation of Terrestrial Heat Flow Data of Mainland China (5th Edition) and relevant published studies, a heat flow distribution map for the Tengchong Block–Longchuan Basin was constructed (Fig. 6). The Tengchong Block as a whole exhibits relatively high heat flow values (75–110 mW/m^2), significantly exceeding the Chinese continental average (61.5 mW/m^2). This feature reflects the active tectonic environment associated with the ongoing collision between the Indian and Eurasian plates. Under this extensional stress regime, lithospheric thinning and mantle heat input jointly contribute to the elevated regional heat flow. In the northern part of the Tengchong Block, localized zones of anomalously high heat flow (>120 mW/m^2) are mainly related to shallow crustal magma chambers and vigorous hydrothermal convection(Zhao et al., 2011). However, these anomaly zones are far from the Longchuan Basin, and the magmatic thermal influence decreases rapidly with distance, exerting little effect on the basin's overall heat flow distribution.

Within the Longchuan Basin, the regional heat flow pattern is broadly consistent with that of the Tengchong Block—higher in the north and lower in the south—but exhibits pronounced local differentiation. Profile analysis reveals that the basin margins are underlain by shallowly exposed metamorphic granite basement with relatively high thermal conductivity (2.95 W/(m·K)), whereas the central depression is filled with thick Neogene sandstone–mudstone sequences exhibiting lower thermal conductivity (1.57–2.03 W/(m·K)). These structural and lithological contrasts, combined with the undulating basement morphology, result in lateral redistribution of heat flow within the basin, forming the characteristic 'high-margin and low-center' thermal pattern.

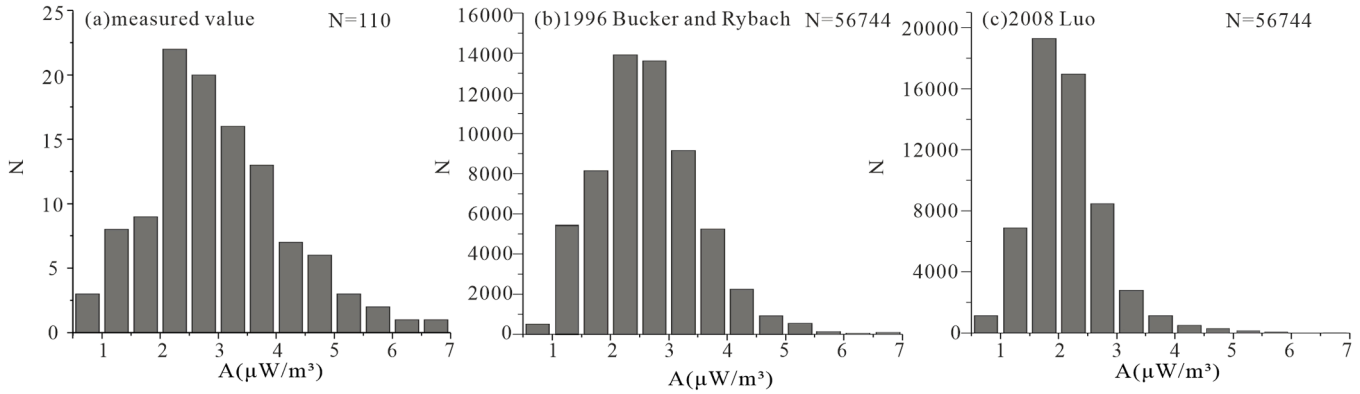

Fig. 5. Statistical chart of heat generation rate in the Longchuan Basin.

Table 2
Thermal properties of rocks in Longchuan Basin.

stratum	lithology	Thermal conductivity W/(m·K)	heat generation rate μW/m^3
N2m	sandstone	2.31 ± 0.03	1.97 ± 0.37
	mudstone	1.55 ± 0.04	
N1n2	siltstone	2.06 ± 0.21	2.22 ± 0.45
	mudstone	1.49 ± 0.12	
N1n1	Silty mudstone	1.60 ± 0.08	2.54 ± 0.52
	siltstone	2.06 ± 0.21	
	Pebbly coarse sandstone	1.61 ± 0.15	
Basement	Mixed gneiss	2.95 ± 0.69	2.01 ± 0.36

3.4. Temperature distribution

Due to the limited number of drilling wells and the relatively shallow drilling depths in the study area, obtaining direct measurements of the deep formation thermal state within the basin is challenging. However, by utilizing the existing temperature measurement curves and data, and considering the structural and stratigraphic distribution in the area, it can be concluded that the primary heat transfer mechanism is still dominated by heat conduction, despite some convection occurring in the shallow strata. Therefore, the heat conduction equation can be applied to estimate the deep ground temperature.

Based on the estimated formation heat generation rate, it was found that the radioactive heat generation rate of the rocks in the study area is relatively uniform. Although local variations exist, the overall trend remains stable. This uniform distribution of heat generation rate results in a temperature gradient that is approximately linear, making the simplified one-dimensional steady-state heat transfer equation a feasible calculation method. The specific equation used is:

$$T(Z) = T_0 + \frac{q_0 Z}{K} - A_0 Z^2 \Big/ (2K) \quad (4)$$

Where $T(Z)$ is the temperature (°C) at depth Z(m), T_0 is the surface temperature (19 °C, which varies between 17–19 °C in the Longchuan area), q_0 is the surface heat flow value (mW/m^2) at the calculation point, K is the weighted average thermal conductivity (W/m·K) of the layer in the 0-Z segment, and A_0 is the average radioactive heat generation rate (μW/m^3) of the rocks in the 0-Z section, calculated layer by layer from the surface to depth using the delamination method.

Using Eq. (4), the formation temperatures at the top of different layers and at various depths were calculated, and a spatial distribution map of temperature was created using the Kriging interpolation method (Fig. 7). The results show that the Neogene formation depth in this area is relatively shallow, leading to generally low formation temperatures. Specifically, the temperature of the Manangba Formation (buried at 300–600 m) is typically below 45 °C, meaning conditions are not yet suitable for the formation of effective low-temperature hydrothermal resources.

The reliability of the calculated temperature field was verified using measured temperature data. The measured temperatures of well L4X indicate that the top of the second member of the Nanlin Formation reaches 44.3 °C, while the calculated temperature using Eq. (4) is 43.2 °C. The measured temperature at the top of the first member of the Nanlin Formation is 54.6 °C, and the corresponding calculated value is 53.2 °C. At the top of the basement, the measured temperature is 83.3 °C, and the calculated temperature is 81.2 °C. These results show that the modeled temperatures are very close to the measured data, with deviations of less than ±2 °C, confirming that the one-dimensional steady-state conductive model can reliably reproduce the actual subsurface temperature distribution.

The temperature of the second member of the Nanlin Formation is influenced by burial depth, exhibiting a trend of "shallow in the northwest and deep in the southeast." In the eastern part, where the burial depth reaches approximately 1250 m, the temperature is about 60 °C, indicating some potential for low-temperature hydrothermal resources. The temperature of the first member of the Nanlin Formation increases as the burial depth rises to 1400–1600 m, with temperatures reaching 70 °C. In some areas at the base of the Nanlin Formation, the burial depth is around 1700–2200 m, with temperatures reaching up to 80 °C, creating favorable conditions for the formation of low-temperature hydrothermal resources.

Despite the relatively low formation temperatures in the shallow thermal reservoirs, their shallow depth significantly reduces development costs, as the thermal reservoir roof is typically located at depths of <1500 m As a result, the shallow geothermal system still holds substantial development potential. For deeper strata, the temperature increases significantly with burial depth, ranging from 64–100 °C at 2000 m to 135–185 °C at 5000 m. The temperature distribution follows a 'low in the middle, high at the edges' pattern, consistent with the geothermal heat flow distribution (Fig. 8). A high-temperature anomaly of 130 °C was observed in the northwest slope zone and the southeast uplift zone at depths between 2000–3000 m. As the burial depth increases further (4000–5000 m), the high-temperature core gradually expands toward the basement uplift area in the northeast, with the peak temperature reaching 185 °C at a depth of 5000 m. Given that the basement lithology is predominantly composed of dense metamorphic rocks, the study area has significant potential for high-quality hot dry rock resources (>150 °C).

3.5. Reservoir-Cap rock combination

The sandstone layers in the study area are mainly developed in the Mangbao Formation and the first and second members of the Nanlin Formation. As shown in the well correlation section (Fig. 9), the thickness of the sandstone body in the first member of the Nanlin Formation varies across different structural positions. Specifically, wells Lc1 and L2 show a larger sedimentary thickness, while well L3 exhibits a smaller thickness, indicating the heterogeneity of the sand body in this region. Overall, the sandstone body is layered and discontinuously distributed, with significant local variations in thickness. The connectivity of the sandstone layer at the base of the first member of the Nanlin Formation is generally good. The sandstone is predominantly interbedded with mudstone, and the mudstone is thick and stable in some areas, which could act as a barrier to fluid migration. However, it also exhibits low thermal conductivity, making it an effective cap rock and conducive to the formation of geothermal resources.

A physical property analysis of 219 rock samples from well Lc1 shows that the porosity of the sandstone layer in the Nanlin Formation ranges from 1.42 % to 34.10 %, with an average of 16.2 % (Fig. 10a).

Table 3
Newly measured terrestrial heat flow data in Longchuan Basin.

Well Name	latitude	longitude	Heat-flow interval top (m)	Heat-flow interval bottom(m)	Temperature gradient (°C/100 m)	Thermal conductivity (W/(m·K)	Thermal conductivity source	Thermal conductivity location	Heat flow value (mw/m^2)	Heat flow quality
L4x	97.93769	24.33069	630	1140	4.58	1.88	Core samples	Actual heat-flow location	86.01	A
Lc1	97.83026	24.24195	0	1610	4.14	1.91	Core samples	Adjacent well	79.34	B

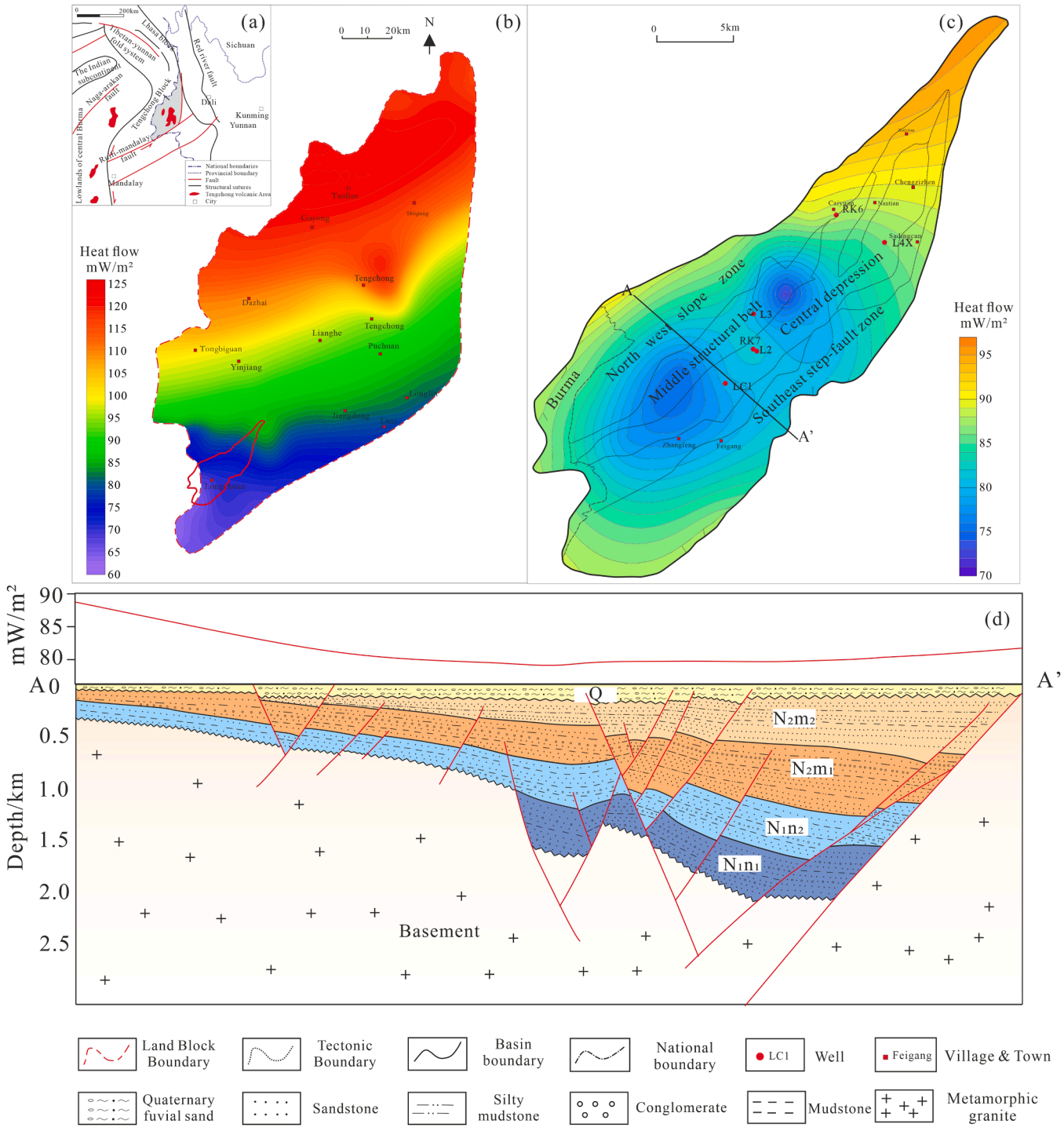

Fig. 6. Heat flow distribution map of Tengchong block and Longchuan Basin.

Among the samples, 10 % are high-porosity reservoirs (porosity > 25 %), and 85 % of the samples have porosity between 5 % and 25 %. Permeability tests on 149 samples indicate that the maximum permeability reached 1000 × 10^{-3} μm², with an average of 52.67 × 10^{-3} μm² (Fig. 10b). Notably, over 20 % of the samples fall within permeability ranges of 0.01 to 0.001 × 10^{-3} μm² and 0.1 to 1 × 10^{-3} μm², showing a bimodal permeability distribution.

The formation temperature analysis reveals that the temperature at the top of the first member of the Nanlin Formation is mostly between 40 and 80 °C, meeting the requirements for hydrothermal resource development. The sandstone reservoir is well-developed, with moderate porosity and permeability, and is interbedded with thick, stable mudstone that provides effective sealing. Additionally, high-angle tectonic fractures and joint networks, formed during multiple tectonic episodes, can be enhanced through artificial stimulation, offering potential for EGS development. In summary, the porous sandstone intervals are favorable for hydrothermal systems, while the fractured, low-permeability zones are suitable for EGS applications.

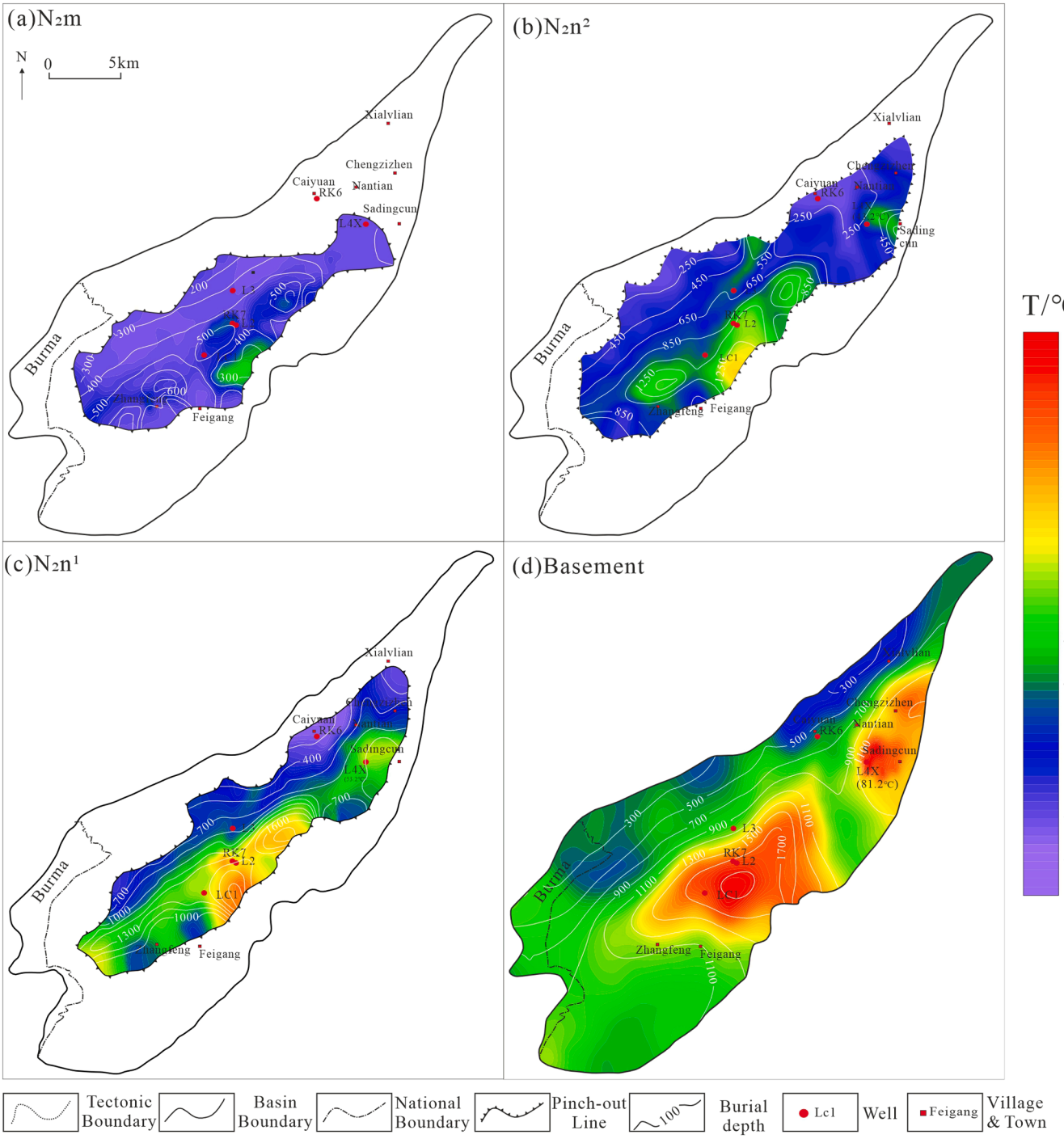

Fig. 7. Temperature distribution of different strata in the Longchuan Basin.

4. Estimation of geothermal resources using the Monte Carlo volumetric method

Based on the stratigraphic and petrophysical characteristics of the Nanlin Formation, which support the development of both hydrothermal systems and EGS, this study applies the volumetric method to quantify their respective resource potential. This method estimates the total heat content in a defined rock volume, including both the solid matrix and pore fluids, using the following equations(5) - (7).:

$$Q_{Total} = Q_R + Q_W \tag{5}$$

$$Q_R = AD(1-\varphi)\rho_R C_R (T - T_0) \tag{6}$$

$$Q_W = AD\varphi\rho_W C_W (T - T_0) \tag{7}$$

Where Q_{Total},Q_R and Q_W represent the total geothermal energy and the heat energy stored in rocks and pore water, respectively. The parameters used in the calculation are as follows:

A(m^2)is the area of the geothermal heat storage.
D(m)is the thickness of the heat storage layer.
ρ_R (kg/m^3) is the density of the geothermal reservoir rock.
ρ_W (kg/m^3) is the density of the geothermal water.
C_R (J/(kg· °C)) is the specific heat capacity of the geothermal reservoir rock.

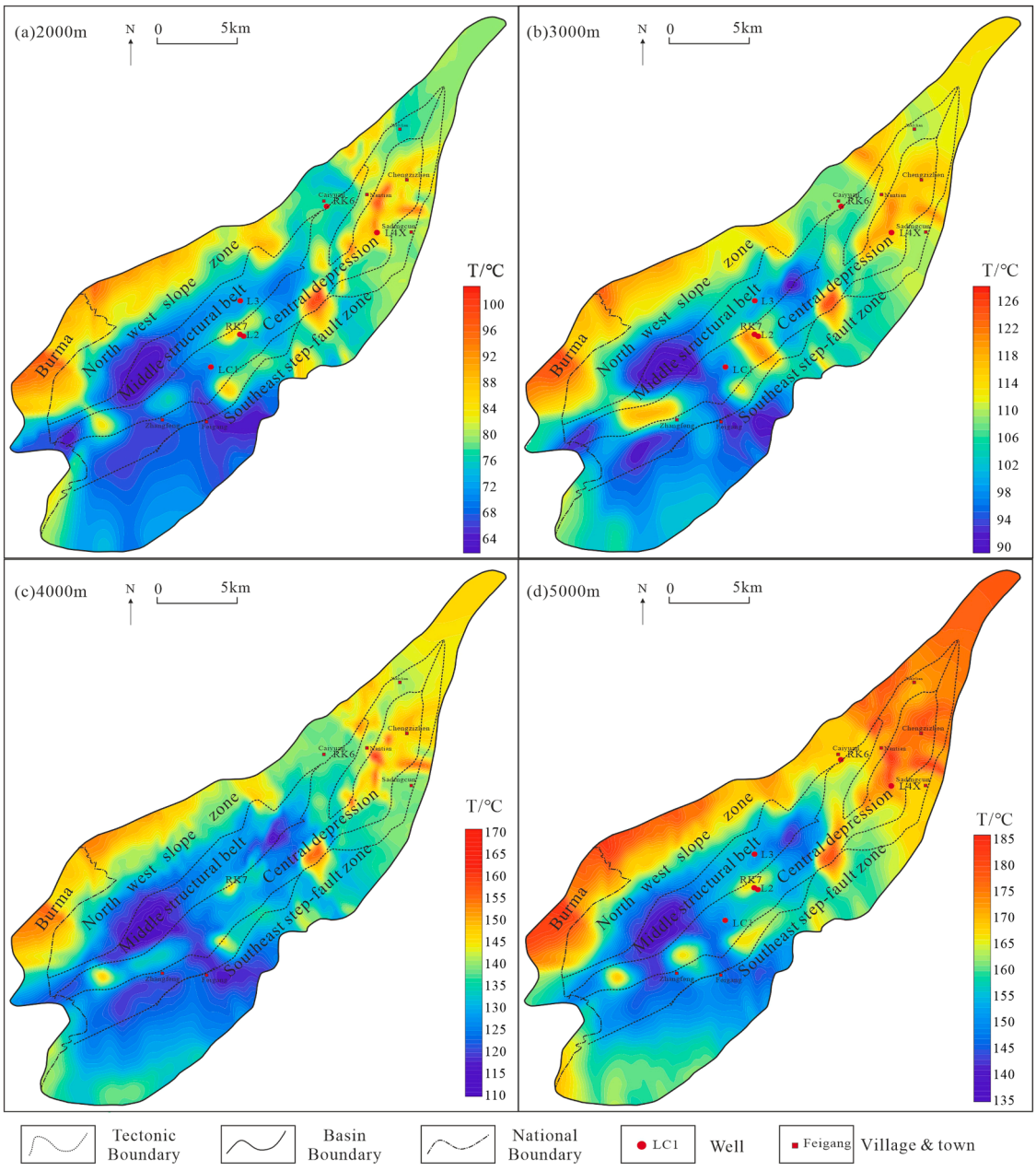

Fig. 8. Temperature distribution map of different buried depths in the Longchuan Basin.

C_W (J/(kg· °C)) is the specific heat capacity of the geothermal water.
Φ(%) is the porosity of the geothermal rock, expressed as a percentage.
T (°C) is the average temperature of the geothermal rock and water within the specified volume.
T_0 (°C) is the reference temperature, which is typically the temperature of the local constant temperature layer.

Due to limited drilling data, complex geological conditions, and significant uncertainty in reservoir parameters, the volumetric method often yields substantial errors when estimating resources in low-exploration areas. The calculation of the volumetric method requires assigning values to key parameters such as reservoir thickness, porosity, and permeability based on regional geological predictions and empirical data. These parameters can vary significantly across regions, directly impacting the accuracy of the estimates. Additionally, thermal reservoirs in low-exploration areas are frequently influenced by tectonic activity, which can cause significant lateral and vertical variations. However, the volumetric method assumes a uniform distribution of reservoirs, making it difficult to accurately capture these complexities. Moreover, traditional volumetric methods typically use a single deterministic value for calculations, disregarding the variability of geological parameters and failing to provide a reasonable error range, leading to large uncertainties in resource quantity estimates (Li et al., 2023). To address these challenges, this study combines the Monte Carlo simulation with the volumetric method, establishes probability distributions for key parameters, and performs large-scale random simulations to quantify the impact of parameter uncertainty on resource assessment, thereby improving the accuracy of the results (Palmer-wilson et al., 2018; Sutopo and Pratama, 2019; Wang et al., 2021).

4.1. *Hydrothermal geothermal resources*

The shallow hydrothermal geothermal resources in the study area

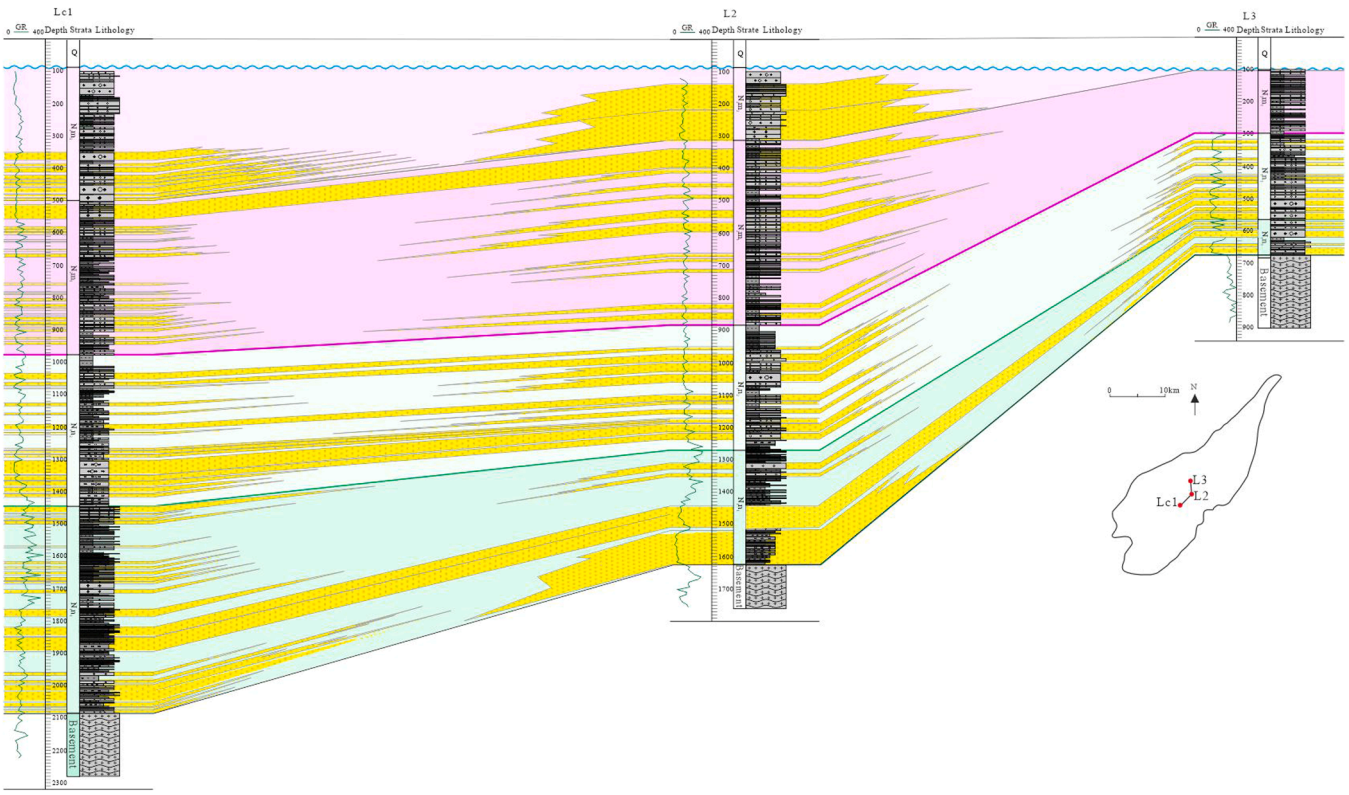

Fig. 9. Longchuan Basin connecting well section.

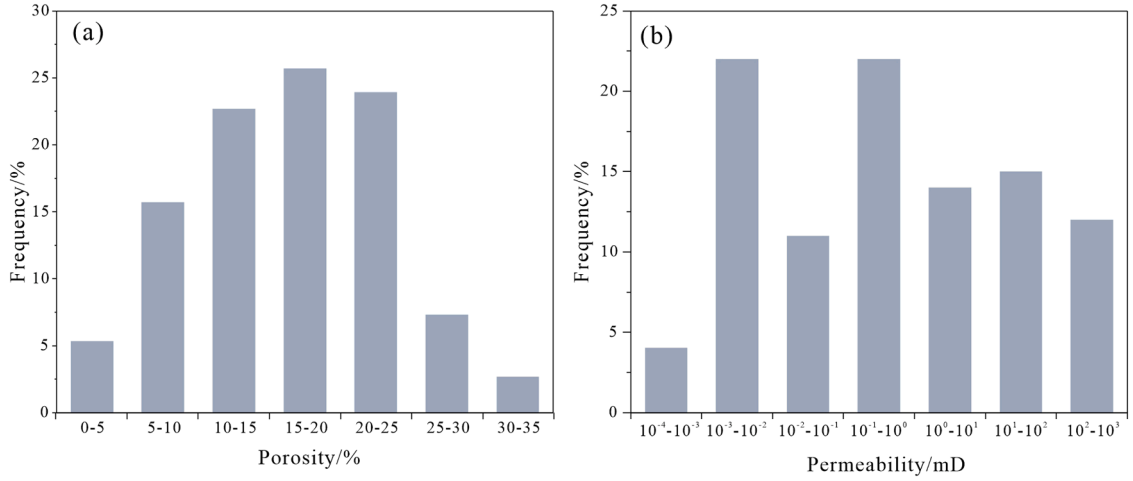

Fig. 10. Physical properties of sandstone from the Nanlin Formation, Longchuan Basin.

are primarily found in the sandstone layer of the first member of the Nanlin Formation. However, due to the shallow sedimentary depth, the formation temperature is generally lower than the lower limit for geothermal water resource development (40 °C), making it unsuitable for direct utilization. As a result, this layer is not considered a target for development. In contrast, the first member of the Nanlin Formation at greater burial depths has a temperature range of 45–65 °C at the top of the formation, which meets the development standards for low-temperature geothermal resources. Based on the temperature distribution map at the top of the first member of the Nanlin Formation, the effective heat storage area is determined to be 17.2 km^2, which indicates strong development potential.

To improve the stability and reliability of the calculations, some key parameters were set to fixed values during the Monte Carlo method-based resource estimation. These include the specific heat capacities of sandstone (826 J/(kg· °C)), mudstone (702 J/(kg· °C)), and water (4200 J/(kg· °C)), as well as the densities of sandstone (2600 kg/m^3) and mudstone (2350 kg/m^3). Considering the heat capacity of the porous media in the sandstone layer, statistical analysis of wells Lc1, L2, and L3 in the Nanlin Formation shows that the variation in the sand-to-land ratio (i.e., the proportion of reservoir sandstones within the effective area) is relatively small, so an average value of 70 % within this range was adopted for calculations. The porosity of the mudstone was assumed to be stable with a fixed value of 15 %.

On the other hand, the thickness (H), temperature (T) in the middle of the first member of the Nanlin Formation, and the porosity (φ) of the sandstone body are significantly influenced by tectonic activities and sedimentary conditions, making it difficult to accurately characterize

their spatial distribution with a single deterministic value. Therefore, prior to Monte Carlo simulation, a systematic statistical analysis was conducted on the distribution characteristics of these parameters based on drilling data, surface temperature calculations, and measured porosity data. Probability distributions were assigned, and the relationships between the parameters were scientifically established.

In statistical modeling, the porosity of the sandstone body (φ) is primarily controlled by sedimentation and diagenesis and is independent of the layer thickness (H) and temperature (T). While there may be some physical correlation between H and T, due to the low exploration degree in the study area, thickness (H) data mainly come from a small number of drilling and geophysical interpretations, while temperature (T) data are based on limited heat flow measurements and borehole temperature calculations, both of which have substantial uncertainty. Thus, probability statistical methods were used to fit the distributions of these parameters, and K-S tests and Chi-square tests were applied to evaluate the fitting effectiveness. The results of the Q-Q diagram show that the thickness (H) of the hot reservoir follows a normal distribution, while the temperature (T) in the middle of the hot reservoir and the porosity (φ) of the sandstone body exhibit triangular distribution characteristics (Fig. 11). Based on these findings, the parameters were randomly sampled using normal and triangular distributions, respectively, in the Monte Carlo simulation, improving the accuracy of uncertainty reflection and enhancing the scientific reliability of the resource assessment.

For resource estimation, the Python programming language, combined with the numpy library for random sampling and the matplotlib library for result visualization, was employed. In the simulation process, 10,000 iterations were performed using a for-loop structure, with each iteration calculating the thermal reservoir resources based on the sampled parameters. The random combinations of these parameters were then analyzed to assess the uncertainty of the geothermal resources, and statistical analysis was performed (Fig. 12). The results indicated a P10 (conservative estimate) of 4.10×10^{14} KJ, a P50 (median estimate) of 8.87×10^{14} KJ, and a P90 (optimistic estimate) of 1.59×10^{15} KJ. The mean estimate was 9.58×10^{14} KJ. The 95 % confidence interval ranged from [2.10×10^{14}, 2.08×10^{15}] KJ. Therefore, the final estimated geothermal resource volume is taken as the P50 value, amounting to 8.87×10^{14} KJ, as it represents a statistically robust and balanced estimate. The study area is underlain by a Mesozoic sandstone-dominated geothermal reservoir. Core analysis results show an average porosity of 16.2 %, with approximately 85 % of samples falling within the 5 %–25 % range, indicating a moderate to good storage capacity. According to the *Specification for Estimation and Evaluation of Geothermal Resources* (DZ/T 0331–2020), a recovery efficiency (RE) of 5 %–10 % is recommended for similar reservoir types. In this study, an empirical value of 10 % is adopted for resource estimation.

The recoverable resource (Q_E) is estimated using the following equation(8):

$$Q_E = Q_{Total} \times RE \tag{8}$$

Based on this, the recoverable resource range can be obtained as [2.10×10^{13}, 2.08×10^{14}] KJ, and the average recoverable resource is 8.87×10^{13} KJ.

To verify the stability and reliability of the calculation results, K-fold cross-validation was conducted, and the calculation error was assessed through multiple training iterations. The cross-validation results showed that the mean relative error was 0.78 %, and the mean standard deviation relative error was 1.79 %. Additionally, outliers were detected using the IQR method and Z-score method, revealing 197 outliers, accounting for 1.97 %, and 87 outliers, respectively (Fig. 13). These outliers were determined to have minimal influence on the calculation results.

To further quantify the influence of each input parameter on geothermal resource estimation, this study employs single-factor sensitivity analysis and the sensitivity index method to assess three key variables: reservoir temperature (T), reservoir thickness (H), and porosity (φ). Assuming all other parameters remain at their average

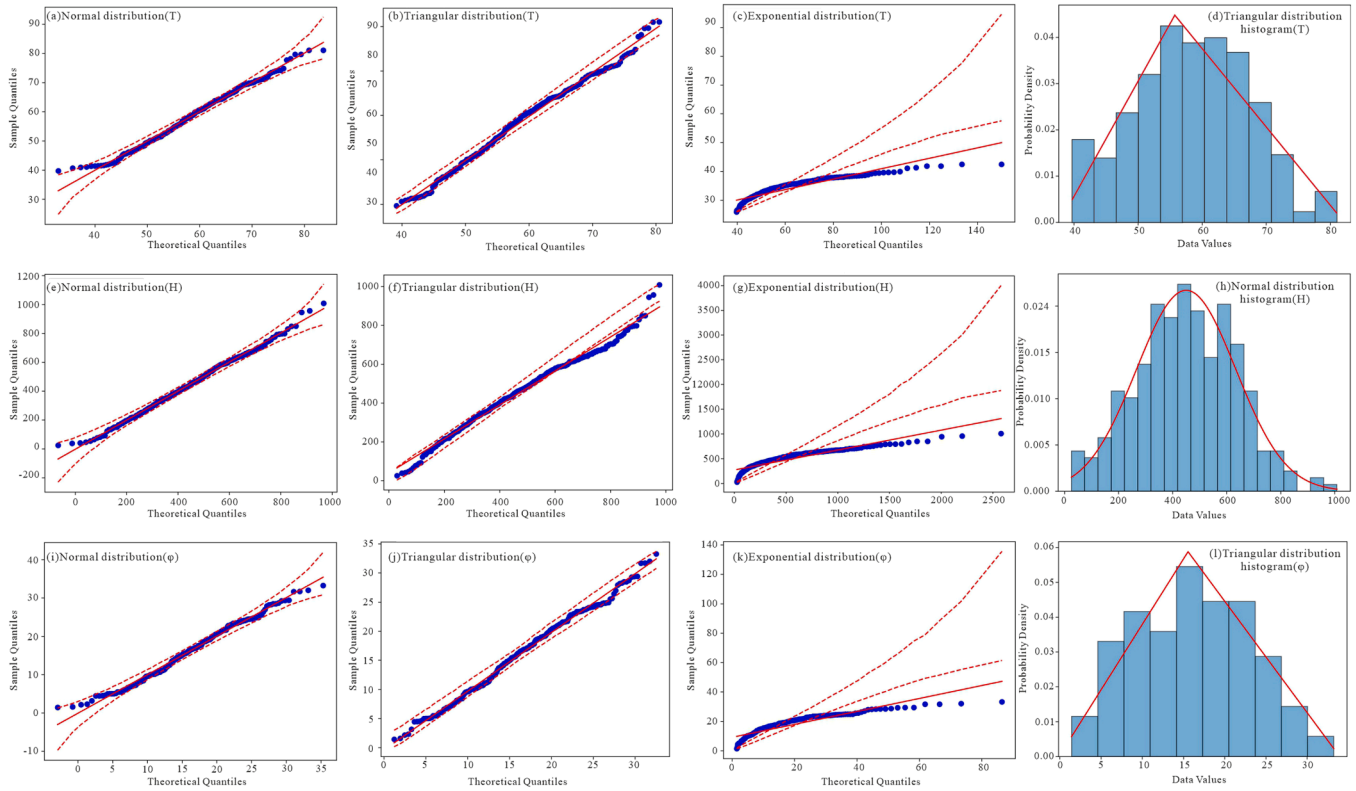

Fig. 11. The distribution of temperature(T) in the middle part of Nanlin Formation, thickness(H) and sandstone porosity parameters(φ) in Nanlin Formation.

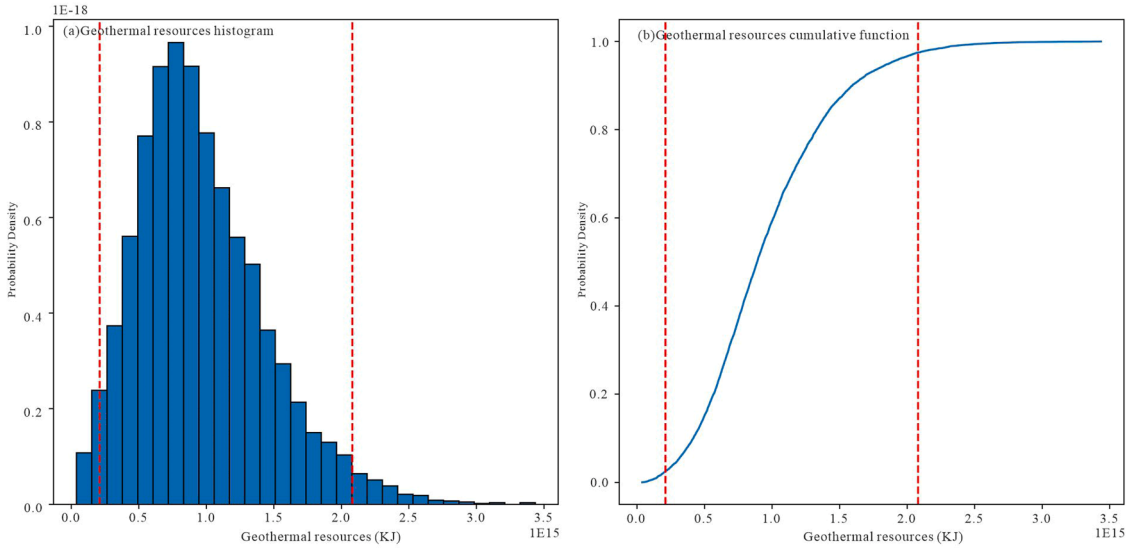

Fig. 12. Evaluation of geothermal resources in the first member of the Nanlin Formation, Longchuan Basin, using the Monte Carlo method.

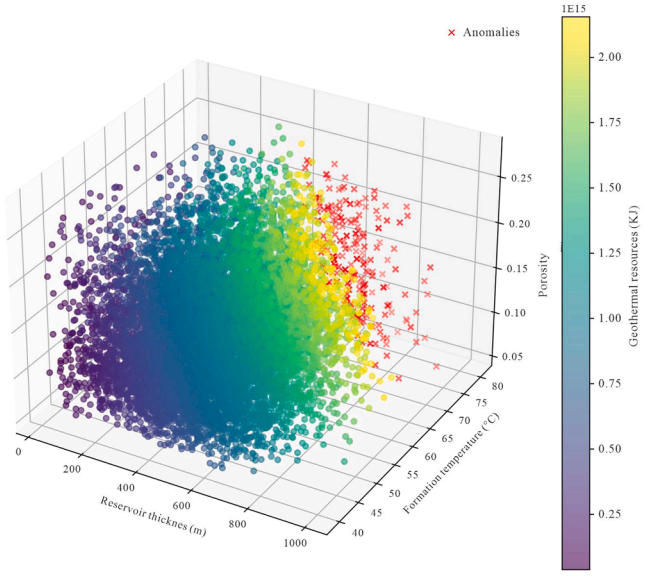

Fig. 13. Scatter map of heat reservoir thickness, formation temperature, porosity and geothermal resources.

values, each variable was individually perturbed within $a \pm 30$ % range to analyze the corresponding variation in estimated resource volumes. The resulting sensitivity curves (Fig. 14) illustrate the response intensity, with steeper slopes indicating higher sensitivity. The results show that resource estimates are most sensitive to temperature changes, followed by reservoir thickness, while porosity has the least impact.

Based on this, the sensitivity index—defined as the percentage change in resource estimate per 1 % change in each parameter—was calculated to provide a more quantitative comparison. The sensitivity index chart (Fig. 15) clearly reveals the relative contribution of each parameter to overall estimation uncertainty. Overall, the acquisition and constraint accuracy of reservoir temperature data play a critical role in reliable geothermal resource evaluation.

4.2. Hot dry rock geothermal resources

Hot dry rock (HDR) geothermal resources primarily occur in dense metamorphic granite strata with burial depths greater than 5000 m, where conduction is the dominant heat transfer mechanism. The heat storage characteristics and temperature distribution of these rocks are critical for assessing the resource potential. Based on the formation temperature distribution map at a depth of 5000 m, this study delineates the effective hot dry rock thermal reservoir area (> 150 °C) in the study area as 125.0 km^2 (125,022,900 m^2). To test the goodness of fit of the formation temperature distribution within this range, Chi-square and K-S tests were applied. The results show that the distribution follows triangular characteristics, and thus, a triangular distribution is used for temperature modeling during the calculation process (Fig. 16).

In terms of parameter setting, due to the technical limitations of the current Enhanced Geothermal System (EGS), the reservoir thickness is set at 300 m, with thermal physical properties such as rock density (2750 kg/m^3) and specific heat capacity (850 J/(kg· °C)) derived from previous research (Jiang et al., 2024). The temperature distribution follows a triangular pattern to represent the deep temperature trend in the study area.

Using these assumptions, 5000 Monte Carlo simulations were performed, yielding results that show the P10 (conservative estimate) is 1.21×10^{16} KJ, the P50 (median estimate) is 1.32×10^{16} KJ, and the P90 (optimistic estimate) is 1.43×10^{16} KJ. The 95 % confidence interval is [1.19×10^{16}, 1.47×10^{16}] kJ, indicating high confidence in the estimated results within this range (Fig. 17). Therefore, the final estimated hot dry rock resource volume is taken as the P50 value, amounting to 1.32×10^{16} KJ. To further estimate the technically recoverable potential of hot dry rock resources, Eq. (8) was applied in conjunction with current technological constraints associated with Enhanced Geothermal Systems (EGS). An empirical recovery rate (RE) of 2 % was adopted for the calculation, in accordance with the typical range of 1 %–2 % recommended by the Evaluation Methods and Estimation Regulations for Geothermal Resources and supported by previous studies (Sun et al., 2022; Wang and Hu, 2012; Yuan et al., 2012). Based on the simulation results, the estimated recoverable resource ranges from 2.30×10^{14} KJ to 3.10×10^{14} KJ, with an average value of 2.64×10^{14} KJ.

To verify the stability of these results, 5-fold cross-validation was performed on the Monte Carlo simulation, showing that the mean relative error was 0.0015 and the mean standard deviation relative error was 0.0106. These findings demonstrate that the method used in this study provides a stable and reliable evaluation of hot dry rock resources.

5. Discussion

The heat flow distribution in the Longchuan Basin is primarily

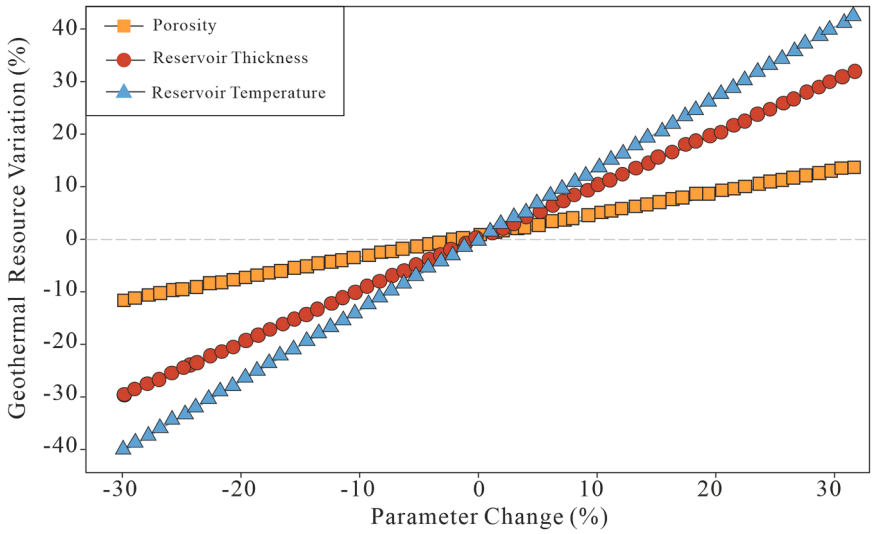

Fig. 14. Sensitivity curves for geothermal resource estimation under ±30 % parameter perturbations.

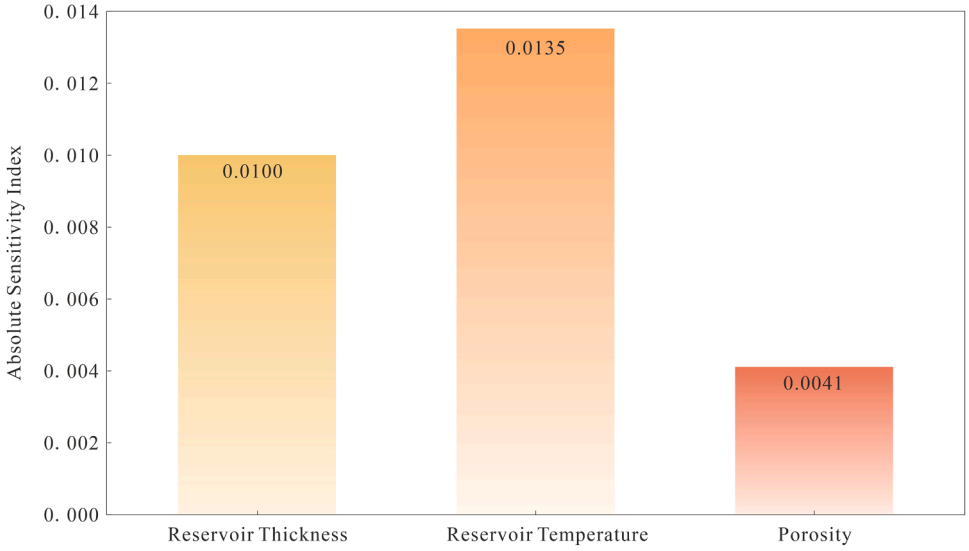

Fig. 15. Comparison of sensitivity indices for reservoir temperature, thickness, and porosity.

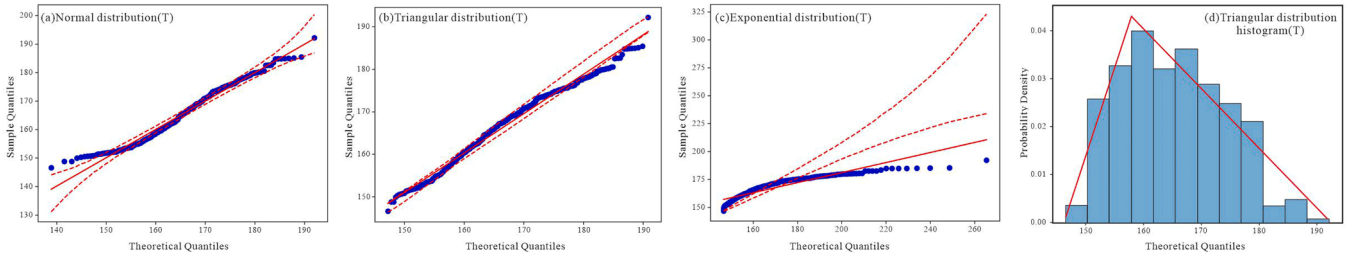

Fig. 16. Test of effective reservoir temperature distribution in hot dry rock buried at 5000 m.

governed by basement undulation and the heterogeneity in the thermal conductivity of the overlying strata, forming a characteristic pattern with higher heat flow at the margins and lower values in the central basin. This configuration contrasts markedly with the high-center and low-margin distribution typical of the Bohai Bay Basin, which is likewise influenced by plate subduction processes. (Rao et al., 2023; Jiang et al., 2016). Although both basins are situated within convergent tectonic settings, heat transfer mechanisms are different. The Longchuan Basin, located within the intracontinental deformation zone of the India–Eurasia collision system, exhibits a relatively thick crust in which conductive heat transfer within the crust predominates. In contrast, the Bohai Bay Basin developed under the subduction and back-arc extensional regime of the Pacific Plate, where lithospheric thinning, fragmentation, and substantial mantle upwelling contribute to a strong mantle-derived heat input (Luo et al., 2026; Wang et al., 2024). At the scale of secondary tectonic units, such as the Jizhong and Jiyang

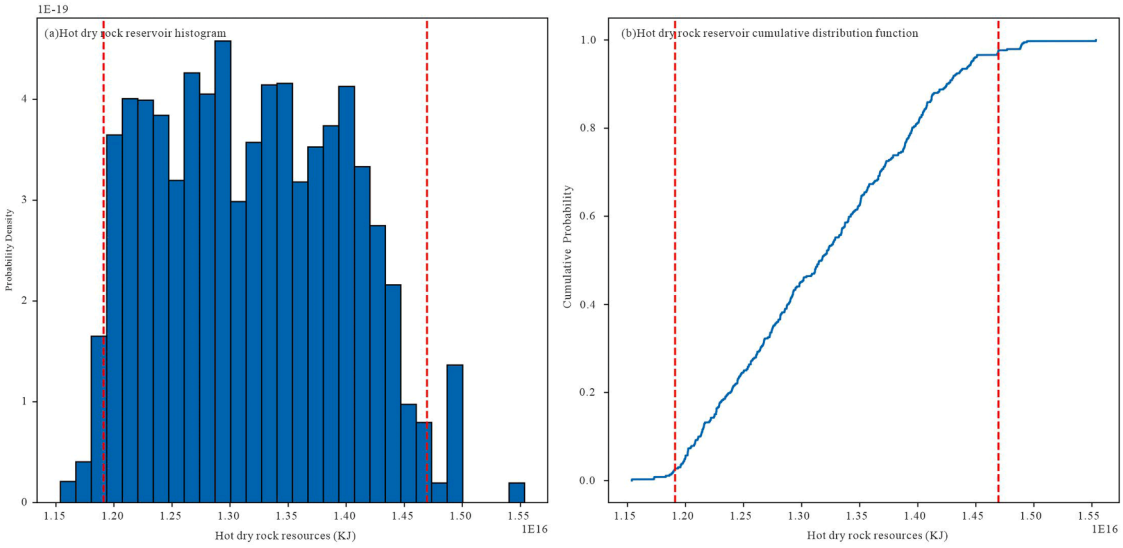

Fig. 17. Evaluation of hot dry rock resources in buried at 5000 m, Longchuan Basin, using the Monte Carlo method.

Depressions within the Bohai Bay Basin, the heat flow distribution exhibits a pattern comparable to that of the Longchuan Basin, characterized by higher heat flow over structural uplifts and lower values in sags (Wang et al., 2021; Zhang et al., 2020). This suggests that in tectonic regions with pronounced basement relief, lateral redistribution of heat flow and variations in thermal conductivity exert a dominant influence on the thermal regime, revealing the multi-scale coupling behavior of geothermal systems.

From the perspective of reservoir structure, the two basins exhibit pronounced differences. In the Bohai Bay Basin, the Neogene–Paleogene sandstone sequences are relatively thick (100–900 m), laterally continuous, and possess good pore connectivity. Deep and large faults serve as conduits for the upward migration of mantle-derived heat, leading to the concentration of geothermal energy within the depressional areas and developing a conductive geothermal system with relatively high reservoir temperatures, where vertical conduction dominates and localized convection is enhanced (Fan et al., 2024; Zuo et al., 2014). In contrast, the first member of the Nanlin Formation in the Longchuan Basin consists of interbedded sandstone and mudstone layers that vary greatly in thickness and exhibit strong heterogeneity. The sandstone bodies are laterally extensive but locally thinned, and the permeability shows a bimodal distribution. The sealing effect of the mudstone layers promotes heat accumulation in the shallow subsurface, giving rise to a shallow hydrothermal geothermal system dominated by conductive heat transfer.

Differences in geological conditions and data availability also determine the applicability and reliability of geothermal resource estimation methods. In the Bohai Bay Basin, dense drilling and well-constrained geological parameters enable the use of the deterministic volumetric method, which generally yields stable results (Qiao et al., 2023; Zhu et al., 2016; Huang et al., 2021). In contrast, the Longchuan Basin is characterized by limited exploration coverage, complex tectonic structures, strong heterogeneity of reservoir properties, and large parameter uncertainties. Therefore, probabilistic uncertainty analysis methods based on statistical simulation are more appropriate. Using the traditional volumetric method, the estimated hydrothermal resource in the first member of the Nanlin Formation is 1.13×10^{19} KJ, while the corresponding hot dry rock resource is 1.32×10^{20} KJ. In comparison, the 95 % confidence intervals derived from a Monte Carlo–based probability distribution model are [2.10×10^{14}, 2.08×10^{15}] KJ and [1.15×10^{16}, 1.55×10^{16}] KJ, respectively. The two methods differ by approximately three orders of magnitude for hydrothermal resources and two to three orders for hot dry rock resources, indicating that the deterministic approach tends to systematically overestimate resource potential in poorly explored regions.

The Monte Carlo method, by quantifying uncertainty through probability distributions, random sampling, and cross-validation (average error <1 %), substantially reduces the sensitivity of individual parameters and improves the robustness and reliability of the results. For areas with complex geology, limited exploration, and pronounced reservoir heterogeneity—such as the Longchuan Basin—the adoption of probabilistic geothermal resource assessment methods provides a more realistic representation of geological uncertainty and resource variability, offering a scientifically sound and scalable approach for geothermal evaluation and development in low-exploration regions.

6. Conclusions

Based on the characteristics of the low exploration degree and high heat flow background in the Longchuan Basin, Yunnan Province, this study quantitatively evaluated hydrothermal and hot dry rock geothermal resources. By analyzing geological structure, geothermal field characteristics, rock thermal properties, and reservoir cover, and combining the Monte Carlo volumetric method, the following key conclusions were drawn:

1. The difference in basement structural morphology and thermal conductivity leads to the lateral redistribution of heat flow, forming a unique heat flow distribution pattern characterized by ‘high at the edge of the basin and low in the center’.
2. The sandstone layer of the first member of the Nanlin Formation is the main reservoir for hydrothermal geothermal resources. The top surface’s buried depth ranges from 1400 to 1600 m, with temperatures between 70–80 °C, offering favorable development conditions. The estimated average hydrothermal resource is 8.87×10^{14} KJ, and with a recovery rate of 10 %, the average recoverable resource is approximately 8.87×10^{13} KJ. The shallow depth significantly reduces development costs, enhancing economic feasibility. At a depth of 5000 m, the underlying metamorphic basement reaches temperatures of 135–185 °C, creating optimal conditions for hot dry rock (HDR) resource accumulation. The estimated average HDR resource is 1.32×10^{16} KJ; assuming a conservative recovery rate of 2 %, the recoverable HDR resource is approximately 2.64×10^{14} KJ.
3. Through Monte Carlo simulation, this study quantified the uncertainties in reservoir thickness, temperature, and porosity. The cross-validation results demonstrated the stability and reliability of

the method, overcoming the accuracy issues associated with traditional volumetric methods in low-exploration areas where data are limited. This method provides a reliable approach for geothermal resource evaluation in similar areas.

CRediT authorship contribution statement

Xiaoxue Jiang: Writing – original draft. **Chuanqing Zhu:** Conceptualization. **Fang Xie:** Conceptualization. **Yuanjin Sun:** Conceptualization. **Qian Cao:** Conceptualization. **Dong Sun:** Conceptualization. **Chaohe Fang:** Conceptualization. **Yonghui Huang:** Conceptualization. **Yaodong Xu:** Conceptualization.

Declaration of competing interest

The authors declare that they have no known competing financial interests or personal relationships that could have appeared to influence the work reported in this paper.

Acknowledgements

This study is supported by the National Key Research and Development Program of China (2021YFA0716003).

Data availability

Data will be made available on request.

References

Bahadori, A., Zendehboudi, S., Zahedi, G., 2013. Retracted: a review of geothermal energy resources in Australia: current status and prospects. Renew. Sustain. Energy Rev. 21, 29–34.
Banwell, C.J., 1963. Thermal energy from the earth's crust. N Z J Geol. Geophys. 6, 52–69.
Bodvarsson, G., 1974. Geothermal resource energetics. Geothermics 3, 83–92.
Bücker, C., Rybach, L., 1996. A simple method to determine heat production from gamma-ray logs. Mar. Pet. Geol. 13, 373–375.
Carlino, S., Somma, R., Troise, C., et al., 2012. The geothermal exploration of Campanian volcanoes: historical review and future development. Renew. Sustain. Energy Rev. 16 (1), 1004–1030.
Chen, B., Zhao, Y., Kuang, P., et al., 1994. Formation mechanism of Longchuan Basin in Western Yunnan. Pet. Nat. Gas Geol. (04), 308–315.
Chen, H., Zheng, F., Song, R., et al., 2024. Geothermal resource assessment and development recommendations for the Huangliu Formation in the central depression of the Yinggehai Basin. Sustainability 16 (16), 7104.
Chen, K., Lin, Y., Shen, W., et al., 2023. Research progress on the origin of Tengchong volcano: geophysical and geochemical studies. Earth Planet. Phys. (Chin. Engl.) 54 (02), 216–230.
Duan, X., Fan, H., Zhang, H., et al., 2019. Melt inclusions in phenocrysts track enriched upper mantle source for cenozoic Tengchong volcanic field, Yunnan Province, SW China. Lithos 324–325, 180-201.
Fan, Y., Duan, Z., Yang, Y., et al., 2024. Impact of reservoir characteristics on the well spacing of sandstone geothermal reservoir: a case study of Jiyang Depression. Hydrogeol. Eng. Geol. 51 (1), 215–223.
Fariña-González, D., García-Afonso, Ó., Delgado-Torres, A.M., 2025. Assessment of geothermal resources for power generation on La Palma Island, Canary Islands. Geothermics 127, 103263.
Gao, Y., Li, G., Liu, Z., et al., 2023. Lower Paleozoic detrital zircon U-Pb geochronological characteristics of the Baoshan Block in Western Yunnan and its constraints on the proto-tethys tectonic evolution. Acta Petrol. Sin. 39 (3), 921–937.
Garg, S.K., Combs, J., 2015. A reformulation of USGS volumetric "heat in place" resource estimation method. Geothermics 55, 150–158.
Huang, Q., Zhang, H., Kang, X., et al., 2020. Geochemical characteristics and circulation processes of geothermal water in Longchuan depression basin. West. Yunnan. Chin. Karst. 39 (06), 793–801.
Huang, X., Zhang, H., Wang, X., et al., 2021. Characteristics and genetic analysis of the Nanle geothermal field in the Bohai Bay Basin. Geol. Sci. Technol. Bull. 40 (5), 71–82.
Jiang, G., Tang, X., Rao, S., Gao, P., Zhang, L., Zhao, P., Hu, S., 2016. High-quality heat flow determination from the crystalline basement of the south-east margin of North China Craton. Journal of Asian Earth Sciences 118, 1–10.
Jiang, X., Zhu, C., Ding, R., et al., 2024. Development prospects of enhanced geothermal systems in the Bohai Bay Basin based on optimized numerical simulation. Coal Geol. Explor. 52 (01), 93–103.
Li, H., Xu, Z., Cai, Z., et al., 2011. Discovery of Indosinian magmatic thermal events within the Tengchong block in Western Yunnan and its geological significance. Acta Petrol. Sin. 27 (07), 2165–2172.
Li, Y., Long, X., Lu, J., 2023. Evaluation of geothermal resources potential in the uplifted mountain of Guangdong Province using the Monte Carlo simulation. Front. Earth Sci.
Liu, B., Liu, Z., 2015. Prospects for uranium exploration in Neogene sandstone-type uranium deposits in Quxi Basin, Yunnan. Sichuan Geol. J. 35 (03), 396–398.
Liu, Y., Zhou, X., Deng, Z., et al., 2015. Hydrochemical characteristics and genesis analysis of the Jifei hot spring in Yunnan, Southwestern China. Geothermics 53, 38–45.
Luo, M., Pan, H., Zhao, Y., et al., 2008. Natural radioactivity logging and its interpretation in the main hole of the Chinese Continental Scientific Drilling Project. Earth Sci. (J. China Univ. Geosci.) (05), 661–671.
Luo, Y., Rao, S., Shi, Y., et al., 2026. The heat accumulation effect enhanced by groundwater convection in Karst Geothermal Systems: a case study of karst geothermal reservoirs in the Jizhong Depression, Bohai Bay Basin, North China. Geothermics 134, 103511.
Muffler, P., Cataldi, R., 1978. Methods for regional assessment of geothermal resources. Geothermics 7 (2), 53–89.
Noguchi, T., 1970. An attempted evaluation of geothermal energy in Japan. Geothermics 2, 474–477.
O'Sullivan, M.J., Pruess, K., Lippmann, M.J., 2001. State of the art of geothermal reservoir simulation. Geothermics 30, 395–429.
Palacios, A., Koon-Koon, R., Miranda-Flores, G., Lewis, S., Castro-Olivera, P.M., Cordova-Lizama, A., Hernandez-Garcia, A.I., 2024. A Monte Carlo-based approach for the evaluation of Mexico's geothermal potential. Renew Energy 223, 120006.
Palmer-wilson, K., Banks, J., Walsh, W., et al., 2018. Sedimentary basin geothermal favourability mapping and power generation assessments. Renew Energy 127, 1087–1100.
Piris, M.A., Urrutia, J., Sosa, R., 2021. Geothermal resource assessment of a low-enthalpy system using volumetric and Monte Carlo simulation methods: a case study in the Neuquén Basin. Argent. Renew. Energy 177, 758–771.
Qiao, Y., Zuo, Y., Tu, S., et al., 2023. Strata temperatures and geothermal resource evaluation in the Dongpu Depression, Bohai Bay Basin, North China. Sci. Rep. 13, 3630.
Rao, S., Xiao, H., Wang, Z., et al., 2023. Geothermal reservoir characteristics and geothermal resource evaluation of Guantao Formation in the Bohai Bay Basin. Nat. Gas Ind. 43 (5), 141–152.
Rybach, L., 1976. Radioactive heat production in rocks and its relation to other petrophysical parameters. Pure Appl. Geophys. 114 (2), 309–317.
Shangguan, Z., Zhao, C., Li, H., et al., 2005. Evolution of hydrothermal explosions at Rehai geothermal field, Tengchong volcanic region, China. Geothermics 34 (4), 518–526.
Sun, M., Wang, R., Guan, Y., et al., 2022. Estimation of hot-dry geothermal resources in Guangxi. J. Jilin Univ. (Earth Sci. Ed.) 52 (4), 1302–1313.
Sutopo, Prabata, W., Pratama, H.B., 2019. The development study of Karaha–talaga Bodas geothermal field using numerical simulation. Geotherm. Energy 7 (1), 21.
Tong, W., Zhang, J., 1981. Characteristics of Geothermal Activities in Xizang Plateau and their Controlling Influence on Plateau's Tectonic Model. Science Publishers Inc., pp. 841–846
Turan, A., Brown, C.S., Shail, R., et al., 2024. Probabilistic assessment of deep geothermal resources in the Cornubian Batholith and their development in Cornwall and Devon, United Kingdom. Geothermics 122, 103081.
Wang, G., Ma, F., Zhang, W., et al., 2024. Dominant heat transfer mechanism in buried-hill reservoirs in North China: a case study in Xiong'an New area. Earth Sci. Front. 31, 52–66.
Wang, J., Hu, S., 2012. Potential evaluation of hot dry rock geothermal resources in mainland China. Sci. Technol. Rev. 30 (32), 25–31.
Wang, Y., Wang, L., Bai, Y., et al., 2021. Assessment of geothermal resources in the North Jiangsu Basin, East China, using Monte Carlo simulation. Energies 14 (2), 259.
Wu, J., Bai, Y., Pu, T., et al., 2020. Identification and significance of the late cambrian granite body in Huguo, Longchuan County, Western Yunnan. Yunnan Geol. 39 (03), 349–358.
Wu, Y., Zhou, X., Wang, M., et al., 2021. Comparison of hydrogeological characteristics and genesis of the Xiaguan hot spring and the Butterfly Spring in Yunnan of China. J. Hydrol. 593, 125922.
Wu, Y., Zhou, X., Zhuo, L., et al., 2023. Structural controls of the Northern Red River Fault Zone on the intensity of hydrothermal activity and distribution of hot springs in the Yunnan-Tibet geothermal belt. Geothermics 109, 102641.
Xiong, C., Jia, X., Yang, X., et al., 2012. LA-ICP-MS zircon U-Pb dating of the Mengmao orocambrian monzogranite in Longling area, Western Yunnan and its tectonic environment. Geol. Bull. China 31 (Z1), 277–286.
Yuan, W., Liu, Z., Ma, F., et al., 2012. Resource potential estimation of hot dry rock in mainland China. Geoscience 33 (5), 807–811.
Zeng, Z., Yang, L., Cui, Y., et al., 2025. Assessment of geothermal waters in Yunnan, China: distribution, quality and driving factors. Geothermics 130, 103323.
Zhang, Q., Liu, Z., Yin, L., 2021. Geochemical characteristics and genesis of geothermal fluids in metamorphic rock areas: a case study of hot springs in Longchuan Basin, Western Yunnan. J. Jilin Univ. (Earth Sci. Ed.) 51 (06), 1838–1852.
Zhang, X., Hu, Q., 2018. Development of geothermal resources in China: a review. J. Earth Sci. 29 (2), 452–467.
Zhang, Y., Feng, J., Luo, J., et al., 2020. Selection direction of hot dry rock in the central and southern Bohai Bay Basin. Earth Sci. Front. 27 (1), 35–47.
Zhang, Z., Li, S., Zhang, F., 1987. Geochemistry of thermal waters in the Tengchong volcanic geothermal area, West Yunnan Province, China. Geothermics 16 (2), 169–179.

Zhao, C., Ran, H., Chen, K., 2011. Present temperature of crustal magma chambers in the Tengchong volcanic area: estimation from carbon isotope fractionation between CO_2 and CH_4 in hot spring gases. Acta Petrol. Sin. 27 (10), 2883–2897.
Zhu, X., Zhang, Q., Liu, Y., 2016. Geothermal resource evaluation of the western Shandong Plain based on the heat storage method. Geol. Sci. Technol. Inf. 35 (4), 172–177.
Zou, G., Mao, Q., Cong, F., et al., 2016. Geochemical characteristics and genesis of dark mafic enclaves in the Mengyang granite body in Western Yunnan. Geol. China 43 (02), 419–431.
Zuo, Y., Qiu, N., Hao, Q., et al., 2014. Present geothermal fields of the Dongpu Sag in the Bohai Bay Basin. Acta Geol. Sin. (Engl. Ed.) 88, 915–930.